

Efficient Cu²⁺, Pb²⁺ and Ni²⁺ ion removal from wastewater using electrospun DTPA-modified chitosan/polyethylene oxide nanofibers

Citation

SURGUTSKAIA, Natalia, Antonio DI MARTINO, Jiří ZEDNÍK, Lenka LOVECKÁ, Eva DOMINCOVÁ BERGEROVÁ, Dušan KIMMER, Jan SVOBODA, Vladimír SEDLAŘÍK, and Kadir ÖZALTIN. Efficient Cu²⁺, Pb²⁺ and Ni²⁺ ion removal from wastewater using electrospun DTPA-modified chitosan/polyethylene oxide nanofibers. *Separation and Purification Technology* [online]. vol. 247, Elsevier, 2020, [cit. 2023-02-02]. ISSN 1383-5866. Available at <https://www.sciencedirect.com/science/article/pii/S1383586620313885>

DOI

<https://doi.org/10.1016/j.seppur.2020.116914>

Permanent link

<https://publikace.k.utb.cz/handle/10563/1009721>

This document is the Accepted Manuscript version of the article that can be shared via institutional repository.

Efficient Cu²⁺, Pb²⁺ and Ni²⁺ ion removal from wastewater using electrospun DTPA-modified chitosan/polyethylene oxide nanofibers

Natalia S. Surgutskaia^{a,*}, Antonio Di Martino^b, Jiri Zednik^c, Kadir Ozaltin^a, Lenka Lovecká^a, Eva Domincová Bergerová^a, Dušan Kimmer^a, Jan Svoboda^d, Vladimir Sedlarik^a

^aCentre of Polymer Systems, University Institute, Tomas Bata University in Zlin, Tr. T. Bati 5678, 760 01 Zlin, Czech Republic

^bResearch School of Chemistry & Applied Biomedical Sciences, Tomsk Polytechnic University, Lenin Av. 30, 634050 Tomsk, Russian Federation

^cDepartment of Physical and Macromolecular Chemistry, Faculty of Science, Charles University in Prague, Hlavova 2030/8, 128 43 Prague 2, Czech Republic

^dInstitute of Macromolecular Chemistry, Czech Academy of Sciences, Heyrovského nam. 2, 162 06 Prague 6, Czech Republic

* Corresponding author. E-mail address: surgutskaya.natalya@yandex.ru (N.S. Surgutskaia).

ABSTRACT

Diethylenetriaminepentaacetic acid-modified chitosan/polyethylene oxide nanofibers (CS-DTPA/PEO NFs) were developed for enhanced heavy metal ion adsorption. These nanofibers were prepared by electrospinning, and their morphology and structure were investigated by scanning electron microscopy (SEM), and Fourier-transform infrared spectroscopy (FTIR), respectively. The ability of CS-DTPA/PEO NFs to removing copper (Cu²⁺), lead (Pb²⁺) and nickel (Ni²⁺) ions from aqueous solutions was tested at room temperature. The effects of [DTPA]/[NH₂] molar ratio, pH and initial concentration of metal ions on their adsorption capacity were investigated to optimize process conditions, using pseudo-first and apparent-second-order, Boyd and intraparticle diffusion models to determine the rate-limiting step of metal ions adsorption. In turn, Freundlich, Langmuir, Temkin and Dubinin-Radushkevich isotherm models were used to describe the experimental data. The results demonstrate a decrease in the ability of CS-DTPA/PEO NFs to adsorb metal ions in the following order: Cu²⁺ > Pb²⁺ > Ni²⁺. The adsorption equilibrium is established after 90 min from the first contact with solutions containing the metal ions, and data are described using the Langmuir isotherm model. The maximal adsorption capacities of CS-DTPA/PEO NFs for Cu²⁺, Pb²⁺ and Ni²⁺ ions were 177, 142, 56 mg g⁻¹, respectively. The stability and reproducibility of CS-DTPA/PEO NFs were determined after five adsorption-desorption tests.

Keywords: Chitosan, DTPA, electrospinning, nanofibers, adsorption, heavy metals ions

1. Introduction

Water resources are extensively used in all stages of industrial production (chemical and electrochemical, among others) and consequently contaminated with heavy metal ions, which are often disposed of in the environment. The presence of heavy metal ions in drinking water, air and soil leads to their gradual accumulation in living organism, thereby causing various diseases, poisoning and mutations [1,2]. Toxic metals ions, such as Pb^{2+} and Ni^{2+} , can inhibit some enzymes, cause oxidative stress (destroying cell membranes) and alter gene expression [3,4]. As a result, different allergic reactions, cancers, and severe effects on the central nervous system of children and on the reproductive system have already been reported [5,6]. In contrast, other metal ions, such as iron, cobalt, copper, manganese, and zinc, are present in the human body and play a key role in several biochemical processes, but when in excess, these elements can be harmful as well [7]. For instance, excess Cu^{2+} is related to some renal diseases, liver dysfunction, stroke, inflammation and cancer [8]. Therefore, environmental protection and remediation systems must be developed to eliminate pollution.

Generally, water purification processes are expensive and time-, reagent- and energy-consuming and hence inconvenient from an economic standpoint [9]. Currently, heavy metals ions are removed from natural waters and industrial effluents through adsorption, which is one of the most prevalent approaches due to its simplicity, cost-efficiency and process control [9]. In this context, a new generation of nano- and micro-adsorbents have been built on inorganic, organic or hybrid materials for their high sorption capacity, stability and reusability [10,11,12,13,14,15]. With such properties, electrospun membranes based on renewable and low-cost biopolymers become thus an interesting choice for wastewater treatment [16,17,18].

Chitosan-based nanofibers and their adsorption properties of heavy metals have been widely investigated [19,20,21]. Biocompatible, biodegradable and non-toxic nature of chitosan together with reactive functional groups such as hydroxyl (-OH) and amino (-NH₂) groups along the backbone, allowing chemical modification or chelation of heavy metals ions, including copper (Cu^{2+}), lead (Pb^{2+}), cadmium (Cd^{2+}) and arsenate (As^{5+}), among others [22,23,24]. For these reasons, chitosan stands out as a highly attractive polymer, which is widely used in various fields of research. However, one of the main drawbacks of chitosan, particularly of low and medium molecular weight chitosan, is their low electrospinnability, which accounts for the low chemical resistance of such fibers in acidic media and for their reduced ability to bind heavy metals [25,26]. Despite these disadvantages, carboxylic (-COOH), sulfo (-SO₃H) and additional amino groups have been introduced into the chitosan backbone to enhance the adsorption ability [27,28] of chitosan fibers, and Ying Lin et al. [29] and H. Yan [30] have demonstrated that chitosan-poly(acrylic acid) or carboxymethylated derivatives have higher adsorption capacity than natural chitosan.

Diethylenetriaminepentaacetic acid (DTPA) and ethylenediamine-tetraacetic acid (EDTA) are well known chelating agents, which form stable complexes with a wide range of metals [31,32]. Hence, chemical bonding to DTPA and EDTA could increase the sorption properties of chitosan-based materials [33,34]. Yet the number of reports related to materials based on the modification of chitosan with DTPA and EDTA remains limited because the high number of reactive carboxyl groups in the structure of acids causes chitosan crosslinking, forming microgels and beads [35,36]. Nevertheless, a recently developed method for the preparation of DTPA-modified chitosan by EDC/NHS crosslinking in TEMED buffer, which avoids the formation of insoluble forms of chit-osan, opens new opportunities for developing various types of DTPA-modified chitosan-based materials [37].

Based on the above, we developed a method for preparing chitosan-DTPA/polyethyleneoxide nanofibers (CS-DTPA/PEO NFs) by electrospinning (**Scheme 1**). These nano fibers were prepared using sets of DTPA-modified chitosan (CS-DTPA) differing in DTPA content. Their adsorption capacity was tested for Cu^{2+} , Pb^{2+} and Ni^{2+} ions, optimizing the pH, contact time and initial metal concentrations. A series of kinetic and equilibrium batch adsorption experiments were also performed to determine the maximum adsorption capacities. Adsorption on CS-DTPA/PEO NFs was also investigated in depth to improve our knowledge on the underlying mechanism and nature of this process.

2. Experimental part

2.1. Materials

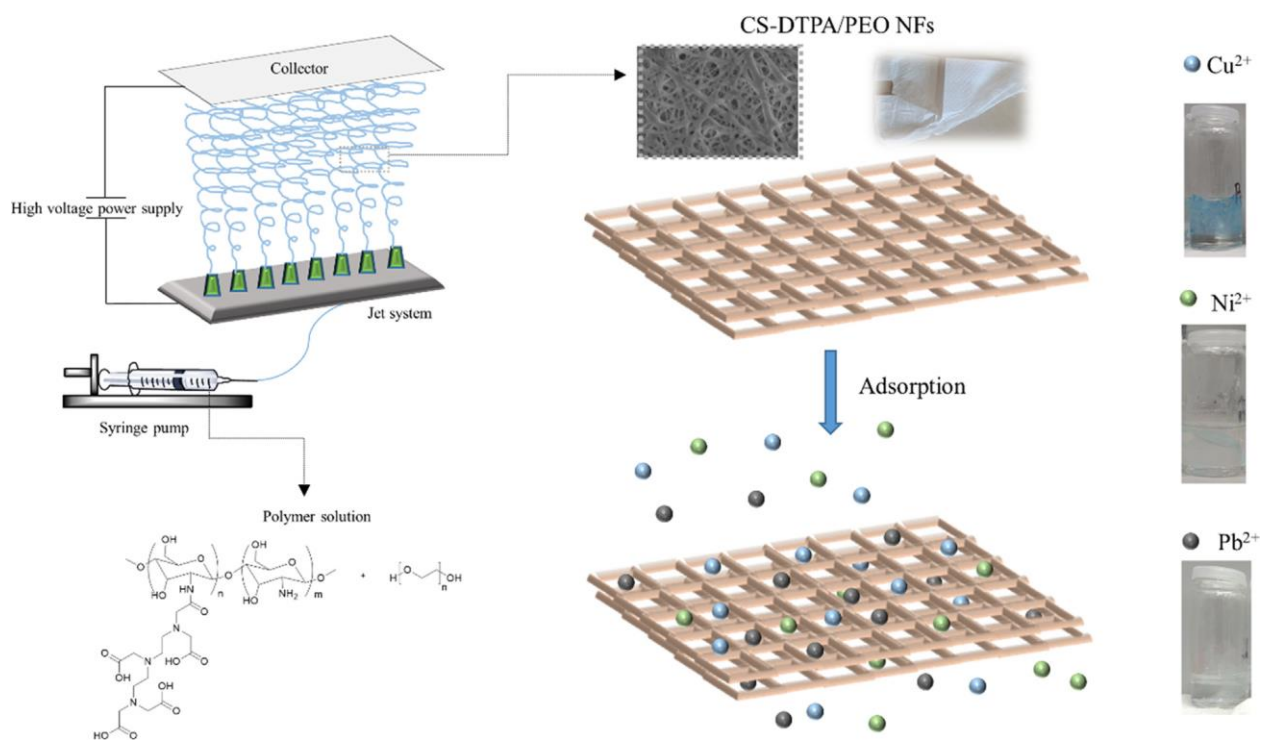
Chitosan (low molecular weight, $M_w = 50\text{-}190$ kDa, deacetylation degree 75-85%), polyethylene oxide (PEO, $M_w = 600\ 000$ g mol⁻¹), Diethylenetriaminepentaacetic acid (DTPA) with purity $\geq 99\%$, N-Hydroxysuccinimide 98% purity, N-(3-Dimethylaminopropyl)-N'-ethylcarbodiimide hydrochloride (EDC) 98% purity, N,N,N',N'-Tetramethyl ethylenediamine (TEMED) with purity $\geq 99.0\%$ and Glutaraldehyde solution (50% in H₂O) were purchased from Sigma-Aldrich. Cuprum (II) sulfate anhydrous with purity $\geq 99\%$ was purchased from Fluka. Nickel (II) sulfate hexahydrate with purity $\geq 98\%$ and lead (II) nitrate with purity $> 99\%$ were purchased from Sigma-Aldrich. Lead, nickel and copper atomic adsorption standards (1000 mg L⁻¹ in 3% nitric acid) were purchased from Agilent Technologies, USA. Potassium carbonate and sodium hydroxide were bought from IPL Lukes, Czech Republic. Ethanol was purchased from Ing. Petr Svec -PENTA s.r.o, Czech Republic. Nitric acid (ACS grade) was purchased from Sigma-Aldrich. Glacial acetic acid analytical grade was purchased from Microchem, Slovakia. All chemicals were used as received without further purification.

2.2. Preparation of DTPA-modified chitosan

DTPA-modified chitosan (CS-DTPA) was prepared by EDC/NHS crosslinking [37]. Briefly, 10 ml of 2% chitosan solution (pH 4.7) was mixed with 10 ml of DTPA solution activated with NHS and EDC ($[\text{NHS}]$ and $[\text{EDC}]/[\text{COOH}] = 1.3$) in TEMED/HCl buffer pH 4.7. The $[\text{DTPA}]/[\text{NH}_2]$ molar ratio ranged from 0.1 to 0.6. The reaction mixture was left standing for 72 h at room temperature, and then the product was recovered and purified by dialysis (MWCO 12 kDa) for 3 days against distilled water. Afterwards, the final product was frozen and dried under vacuum.

2.3. Preparation of CS-DTPA/PEO and CS/PEO nanofibers

The electrospun solution was prepared as follow: a 1.5% CS-DTPA solution in 72% w/w acetic acid was mixed with a 5% w/w PEO solution in 72% w/w acetic acid under stirring overnight to obtain a transparent solution with a 70:30 CS-DTPA/PEO ratio.



Scheme 1. Schematic illustration of preparation and adsorption properties of CS-DTPA/PEO NFs.

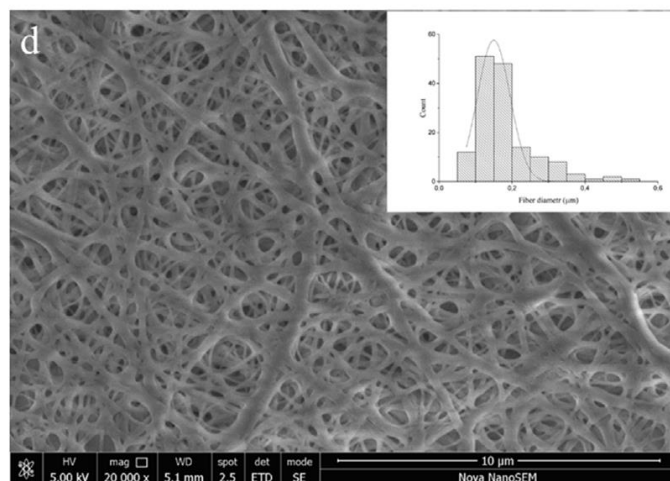
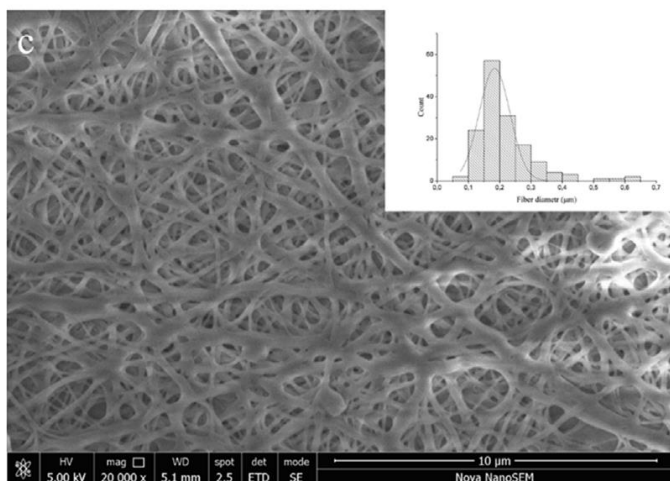
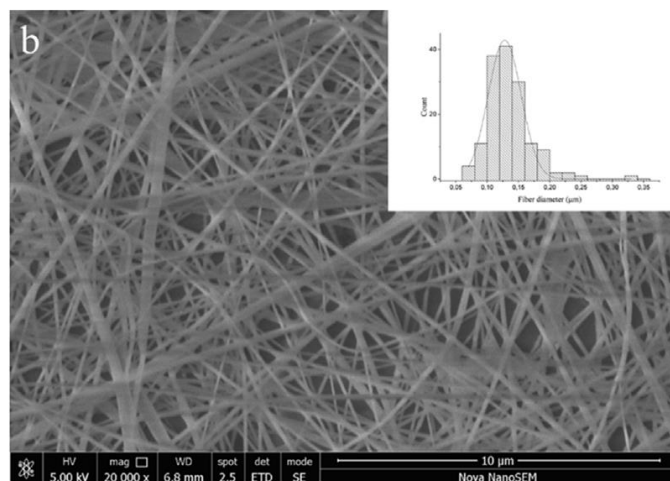
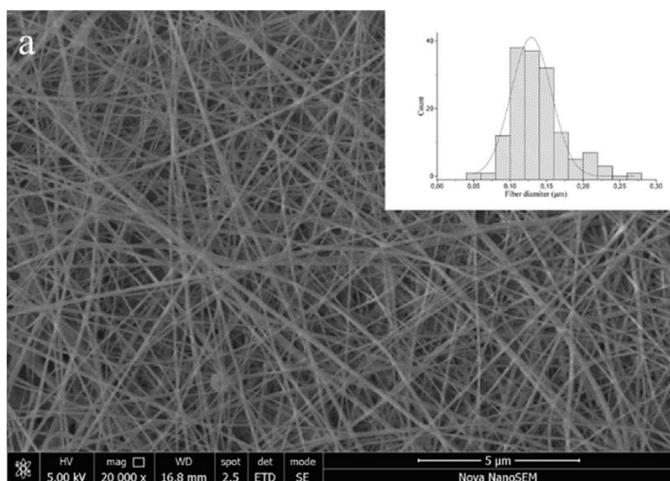


Fig. 1. SEM images and size distribution of pre- and post-stabilized CS/PEO (a-c) and CS-DTPA/PEO (b-d) nanofibers, respectively.

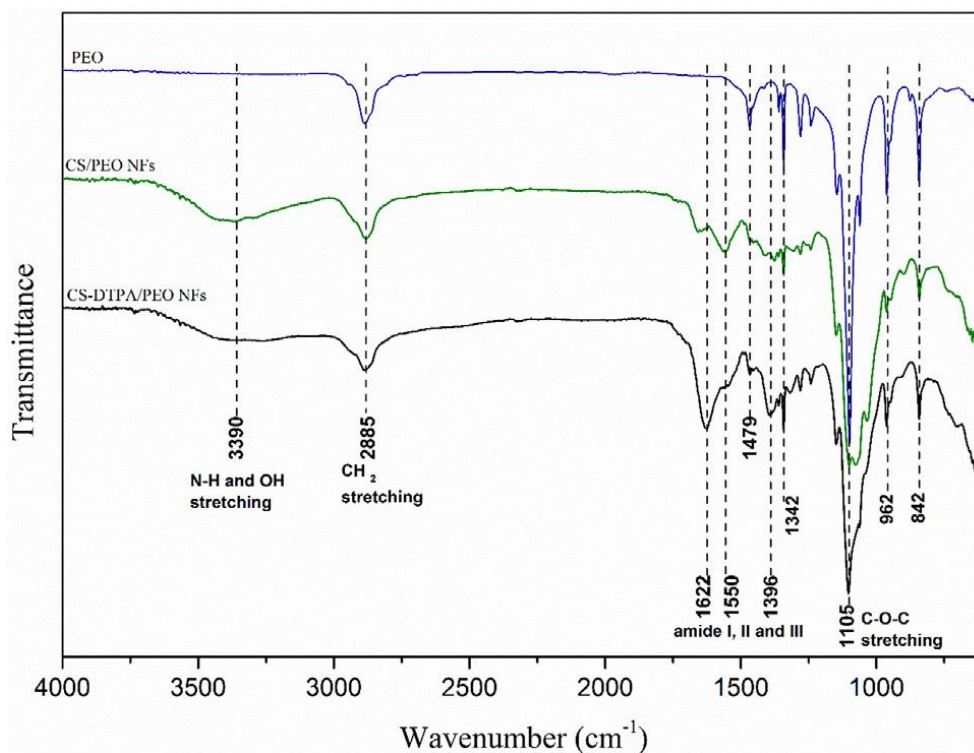


Fig. 2. ATR-FTIR spectra of PEO (blue), stabilized CS/PEO (green) and CS-DTPA/PEO NFs (black).

Electrospinning was performed on a laboratory electrospinning equipment SpinLine 40 SPUR (Czech Republic). The CS-DTPA/PEO (70:30) was loaded in a 20 ml plastic syringe connected to an 8-nozzle jet system. The solutions were electrospun with an applied voltage of 40 kV, the tip-collector distance was 15 cm, and the flow rate of 0.01 ml min⁻¹ was regulated using a syringe pump. Nanofibers were collected on a vertically disposed polypropylene spun bond support (400 250 mm) with a basic weight of 30 g m⁻².

The resulting nanofiber membrane was stabilized by crosslinking under 5% glutaraldehyde vapor for 6 h and then treated with a 1% glycine solution for 4 h and 1 M K₂CO₃ for another 12 h. Afterwards, the membrane was washed with distilled water and dried in a drying chamber at 40 °C for 24 h.

The same procedure was used to prepare the non-modified CS/PEO nanofibers mat.

2.4. Characterization of CS-DTPA and CS-DTPA/PEO and CS/PEO nanofibers

The structure of CS-DTPA was confirmed by ¹H NMR (Varian Unity Inova 400 MHz), using deuterium oxide (Aldrich) (0.6 ml) and adding deuterium hydrochloric acid in deuterium oxide (10 μL) and 1 μL of t-Butanol-OD as a reference standard (δ 1.23 ppm). Spectra were deciphered by first-order analysis. FTIR spectra in the 600-4000 cm⁻¹ range were recorded on an FTIR Spectrometer (Nicolet iS5, Thermo Scientific) equipped with ATR (Ge crystal, 64 scan 4 cm⁻¹) to determine the main functional groups in the structure of raw materials and CS-DTPA/PEO and CS/PEO nanofibers. Morphology and surface

composition were investigated under a scanning electron microscope (NANOSEM 450 FEI, Hillsboro, OR, USA) operated at 5 kV under 90 Pa pressure in a water vapor environment. ImageJ 1.52a (developed by National Institutes of Health) was used to calculate the average diameter and size distribution of nanofibers based on SEM photos taking 150 measurements per sample. X-ray photoelectron spectroscopy (XPS) measurements were carried out with a K-Alpha⁺ spectrometer (ThermoFisher Scientific, East Grinstead, UK). The samples were analyzed using a micro-focused, monochromated Al K α X-ray source (400 μ m spot size) at an angle of incidence of 30° (measured from the surface) and an emission angle normal to the surface. The kinetic energy of the electrons was measured using a 180° hemispherical energy analyzer operated in the constant analyzer energy mode (CAE) at 200 eV and 50 eV pass energy for the survey and high resolution spectra respectively. Data acquisition and processing were performed using Thermo Advantage software. The XPS spectra were fitted with Voigt profiles obtained by convolving Lorentzian and Gaussian functions. The analyzer transmission function, Scofield sensitivity factors, and effective attenuation lengths (EALs) for photoelectrons were applied for quantification. EALs were calculated using the standard TPP-2 M formalism.

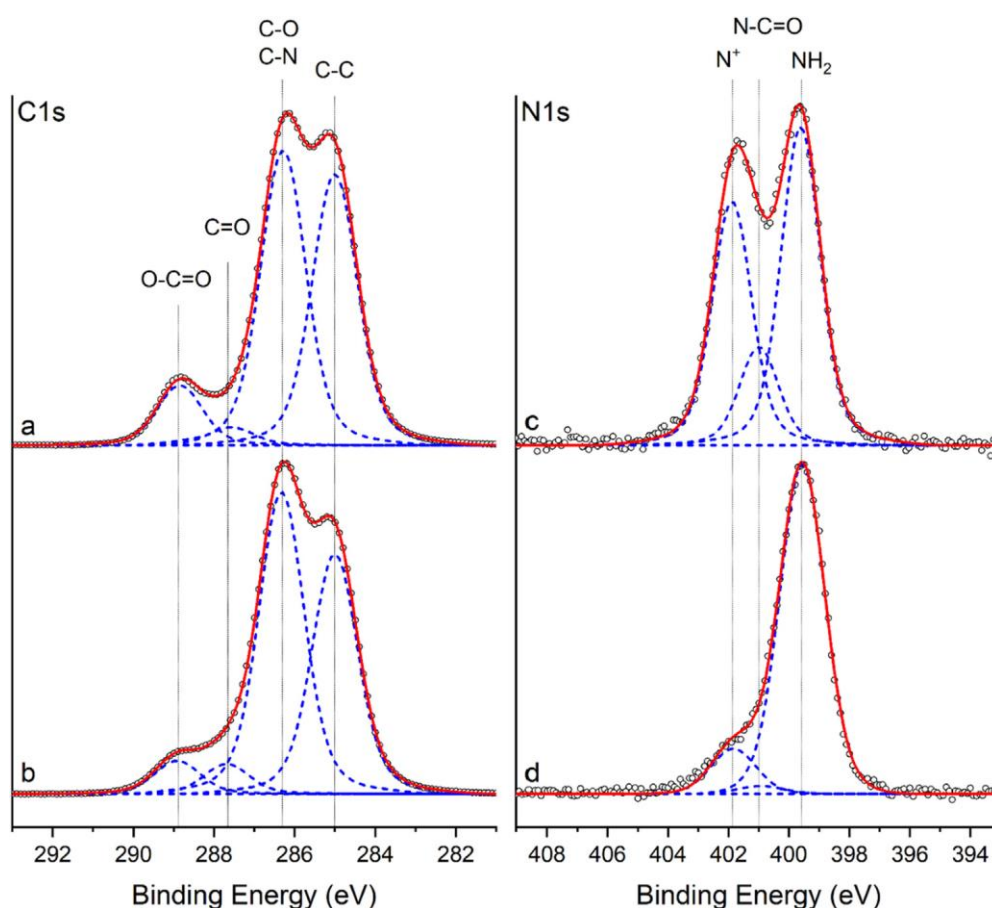


Fig. 3. High-resolution C 1 s and N 1 s XPS spectra of CS-DTPA/PEO (a, c) and CS/PEO (b, d) nanofibers. Measured spectra are presented with open circles, while their corresponding fitted envelopes are presented with red lines. The individual contributions of different functional groups are represented with blue lines.

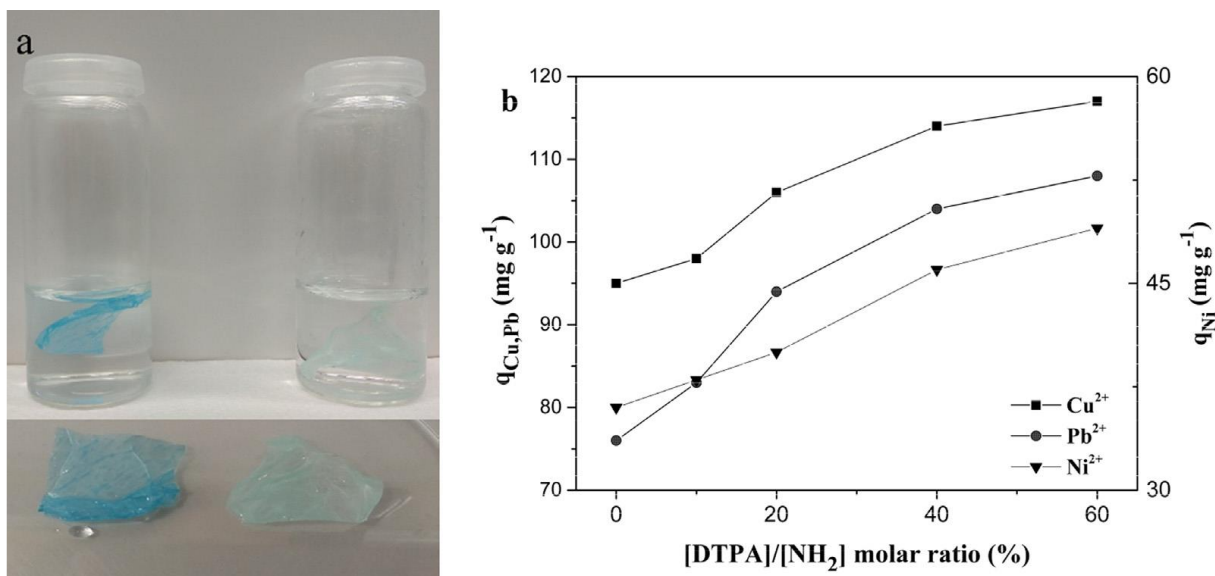


Fig. 4. (a) CS-DTPA/PEO NFs after Cu²⁺ (right) and Ni²⁺ (left) ions adsorption, (b) Plot of the amount of Cu²⁺, Pb²⁺ and Ni²⁺ ions (q) adsorbed on CS-DTPA/PEO NFs vs. [DTPA]/[NH₂] molar ratio. All samples contained 20 mg CS-DTPA/PEO NFs, and the initial metal ions concentration was 300 mg L⁻¹. The amount of metal ions was measured after 120 min of contact under stirring at 150 rpm.

All spectra were referenced to the C 1 s peak of hydrocarbons at 285.0 eV. The BE scale was controlled by the well-known position of the photoelectron C-C and C-H, C-O and O-C = O C 1 s peaks of polyethylene terephthalate and Cu 2p, Ag 3d, and Au 4f peaks of metallic Cu, Ag and Au, respectively. The BE uncertainty of the reported measurements and analysis is in the range of ± 0.1 eV.

2.5. Adsorption experiments

All adsorption experiments were performed at room temperature under continuous stirring (150 rpm) using a fixed amount of adsorbent (20 mg of CS-DTPA/PEO or CS/PEO NFs). The concentrations of Cu²⁺, Pb²⁺ and Ni²⁺ metal ions in the solutions before and after adsorption experiments were determined by Flame atomic absorption spectroscopy (Flame AAS, Duo 240FS/240Z UltrAA, Agilent Technologies, USA) at wavelengths of 324.8, 283.3 and 353.2 nm, respectively. The AAS calibration was performed using Cu²⁺, Pb²⁺ and Ni²⁺ ion standard solutions in the concentration ranges of 1-20, 5-75, 5-80 mg L⁻¹, respectively.

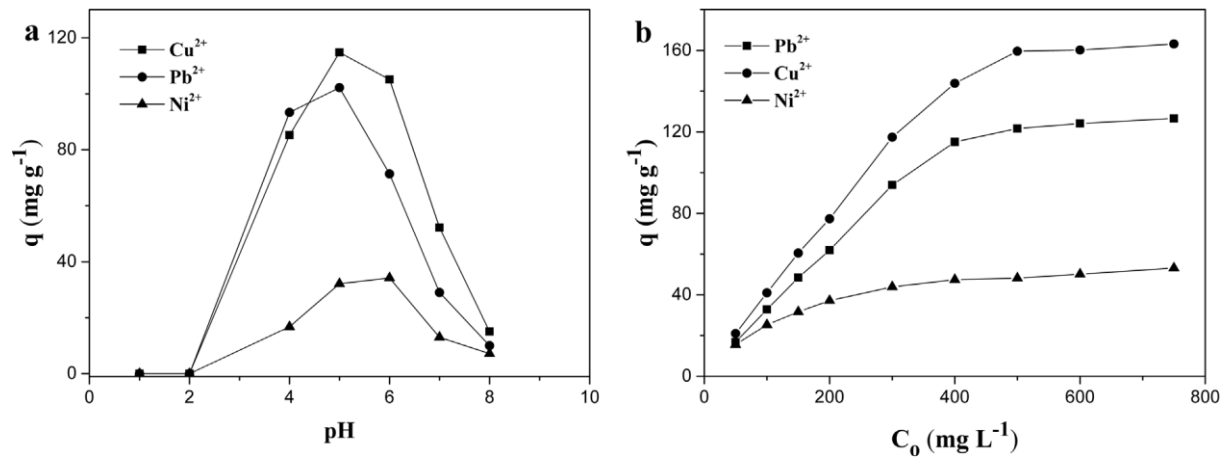


Fig. 5. (a) Cu²⁺, Pb²⁺ and Ni²⁺ ions adsorbed on NFs (q_t) vs. pH (20 mg CS-DTPA/PEO NFs with 0.4 [DTPA]/[NH₂] molar ratio; 300 mg L⁻¹ initial metal ion concentration). (b). Cu²⁺, Pb²⁺ and Ni²⁺ ions adsorbed on NFs vs. initial metal ions concentration (20 mg CS-DTPA/PEO NFs with [DTPA]/[NH₂] molar ratio 0.4, pH 5 for Cu²⁺ and Pb²⁺ and pH 6 for Ni²⁺ ions). The amount of metal ions was measured after 120 min of contact under stirring at 150 rpm.

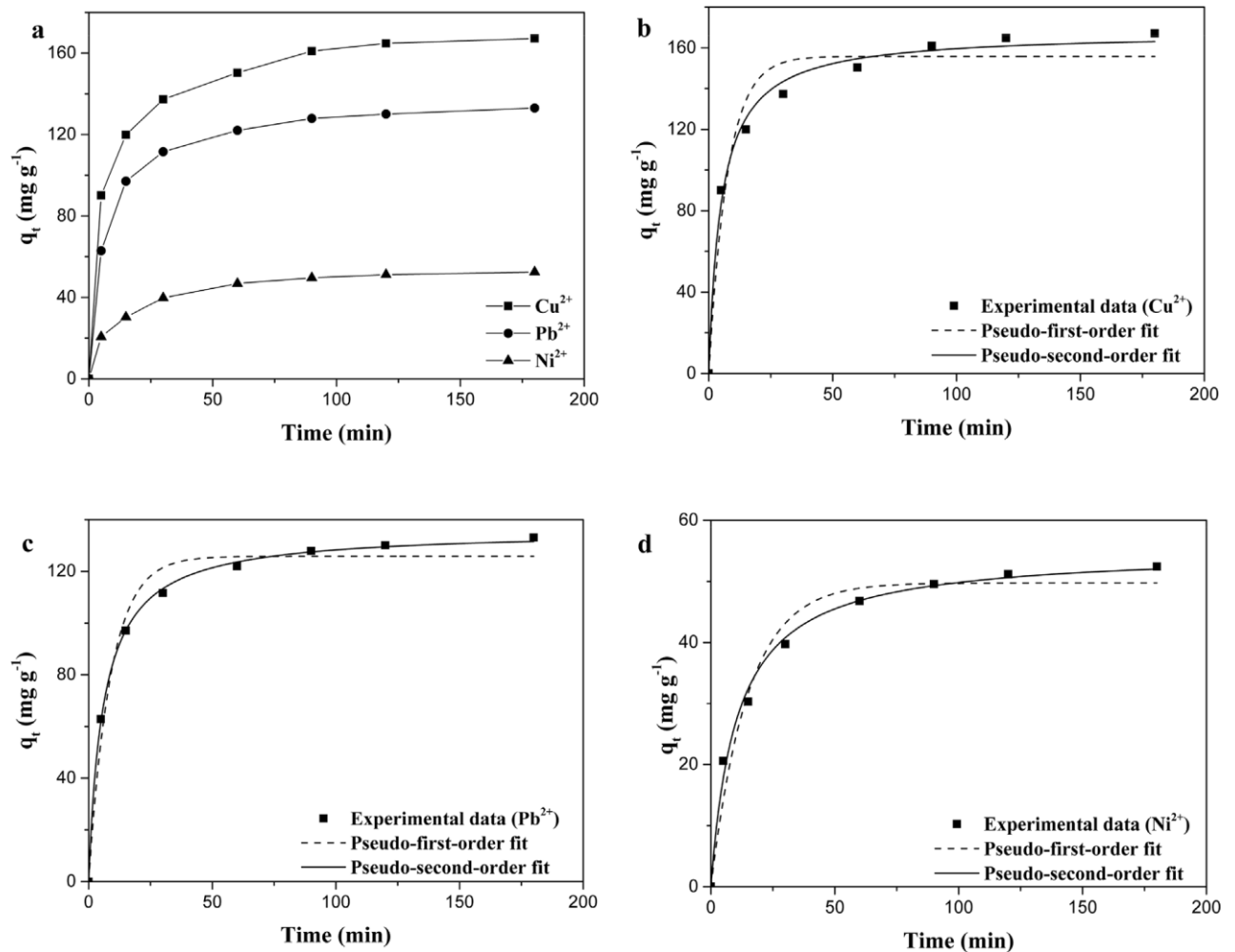


Fig. 6. (a-d) Amount of Cu²⁺, Pb²⁺ and Ni²⁺ adsorbed on NFs (q_t) vs. time (20 mg CS-DTPA/PEO NFs, initial ions concentrations 500 mg L⁻¹, stirring rate 150 rpm). (b-d) Experimental kinetic data fitted using pseudo-first-order and pseudo-second-order kinetic models.

The amount of Cu^{2+} , Pb^{2+} and Ni^{2+} adsorbed, separately, on the nanofibers was calculated as follows [38,39]:

$$q_t = \frac{(C_0 - C_{eq}) * V}{m}, (\text{mgg}^{-1}) \quad (1)$$

where C_0 is the initial concentration of metal ions (mg L^{-1}), whereas C_{eq} represents the concentration at equilibrium (mg L^{-1}); V is the volume of the solution containing the metals (L), and m is the weight (g) of the nanofibers.

2.5.1. Adsorption kinetics evaluation

Kinetic adsorption experiments were performed in parallel using solutions with an initial Cu^{2+} , Pb^{2+} and Ni^{2+} ion concentration of 500 mg L^{-1} . After 5, 15, 30, 45, 60, 90, 120 and 180 min of contact with the nanofibers, the concentration of the metal ions was determined.

Table 1 Correlation coefficient (R^2), kinetic parameters (adsorption capacity (q_e) and rate constant (k_1 , k_2)) of Cu^{2+} , Pb^{2+} or Ni^{2+} adsorption on CS-DTPA/PEO NFs observed using pseudo-first-order and pseudo-second order models.

Metal ions	Pseudo-first-order model			Pseudo-second-order model		
	$q_e(\text{mg g}^{-1})$	$k_1(\text{min}^{-1})$	R^2	$q_e(\text{mg g}^{-1})$	$k_2(\text{g mg}^{-1} \text{ min}^{-1})$	R^2
Cu^{2+}	156	0.16	0.95	168	0.0012	0.99
Pb^{2+}	126	0.13	0.98	136	0.0012	0.99
Ni^{2+}	50	0.08	0.97	55	0.0017	0.99

pseudo-second-order kinetic, Boyd and intraparticle diffusion models, using the following equation [39]:

$$q_t = q_e (1 - e^{-k_1 t}) \quad (2)$$

$$q_t = \frac{q_e^2 k_2 t}{1 + q_e k_2 t} \quad (3)$$

$$-\ln(1 - F) = k_b t \quad (4)$$

$$q_t = K_i t^{1/2} + C_w \quad (5)$$

where q_t and q_e are adsorption capacities at time t (min) and equilibrium (mg g^{-1}), k_1 and k_2 are pseudo-first-order and pseudo-second-order rate constants, F is the solute adsorbed fraction at various times t , k_b is the film diffusion rate constant (min^{-1}), K_i is the intraparticle diffusion rate constant, C_w is the

intercept that confirms the existence of film diffusion and is related to the thickness of the boundary layer. Nonlinear fitting was used to determine the appropriate values of q_e , k_1 , k_2 [40].

2.5.2. Adsorption equilibrium studies

The equilibrium adsorption studies were performed as follow: nano fibers were immersed in 10 ml of solution containing Cu^{2+} , Pb^{2+} and Ni^{2+} ions at variable concentrations; 50, 100, 200, 300, 400, 500, 600, 750 mg L^{-1} . The amount of adsorbed metal ions was determined after 90 min of exposure.

The experimental data were fitted using Langmuir and Freundlich equations, respectively [39,41]:

$$q_e = \frac{q_{\max} K_L C_e}{1 + q_{\max} K_L C_e} \quad (6)$$

$$q_e = K_F C_e^{1/n} \quad (7)$$

where q_e and q_{\max} are equilibrium and maximum metal uptake capacities (mg g^{-1}), C_e is equilibrium metal ion concentration in the solution (mg L^{-1}), K_L is the equilibrium constant of the Langmuir model (L mg^{-1}), and K_F and n are the Freundlich constants, which represent adsorption capacity and intensity, respectively.

Table 2 Correlation coefficient of fitted curves (R^2) and rate constants (k_b , K_1 , K_2) of Cu^{2+} , Pb^{2+} or Ni^{2+} ion adsorption on CS-DTPA/PEO NFs calculated according to the Boyd and intraparticle diffusion kinetic models.

Metal ion	Boyd model			Intraparticle diffusion model			
	$k_b(\text{min}^{-1})$	Intercept	R^2	$K_1(\text{mg g}^{-1} \text{min}^{-0.5})$	R^2	$K_2(\text{mg g}^{-1} \text{min}^{-0.5})$	R^2
Cu^{2+}	0.028	0.74	0.99	14.6	0.96	2.8	0.75
Pb^{2+}	0.017	1.00	0.93	15.0	0.90	1.9	0.89
Ni^{2+}	0.015	0.73	0.91	5.9	0.99	1.0	0.89

To describe the nature of the adsorption process, the equilibrium data were processed using the Dubinin-Radushkevich and Temkin isotherms models [26,42]:

$$\ln q_e = \ln q_{\max} - \beta_{DR} \varepsilon^2 \quad (8)$$

$$q_e = \frac{RT}{b} \ln K_T + \frac{RT}{b} \ln C_e \quad (9)$$

where q_e and q_{\max} are equilibrium and maximum metal uptake capacities (mmol g^{-1}), C_e is equilibrium the metal ion concentration in the solution (mmol L^{-1}), β_{DR} is the Dubinin-Radushkevich constant ($\text{mol}^2 \text{J}^{-2}$), ε is the Polanyi potential ($\varepsilon = RT \ln(1 + 1/C_e)$), R is the molar gas constant ($8.314 \text{ J mol}^{-1} \text{ K}^{-1}$), T is absolute temperature (K), b is the Temkin coefficient, which is related to sorption heat (J mol^{-1}), and K_T is the Temkin isotherm constant. The K_T , q_{\max} and b , β_{DR} were calculated from the intercepts and slopes of fitting curves, respectively. Based on β_{DR} , the mean adsorption energies E (kJ mol^{-1}) were calculated according to the following equation [26]:

$$E = \frac{1}{\sqrt{2\beta_{DR}}} \quad (10)$$

2.6. Competitive adsorption study

The competitive adsorption study was performed in 50 ml of Cu^{2+} , Pb^{2+} and Ni^{2+} mixed solution (200 mg mg L^{-1} , $\text{pH} = 5$) and 100 mg of CS-DTPA/PEO or CS/PEO NFs. The amount of each adsorbed metal ion was determined after 90 min of experiment.

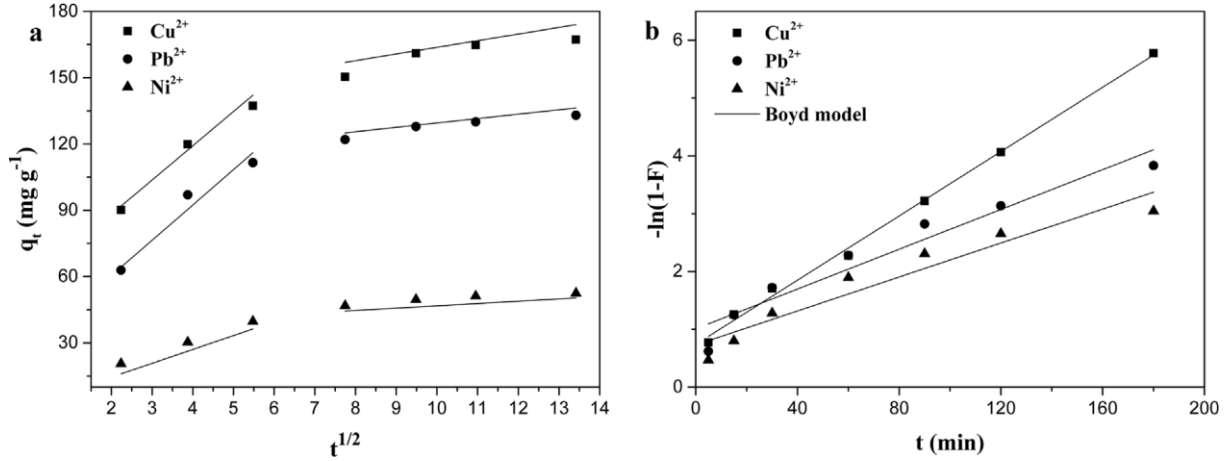


Fig. 7. (a) Amount of Cu^{2+} , Pb^{2+} and Ni^{2+} adsorbed on NFs (q_t) vs. $t^{1/2}$ time, fitted using the intraparticle diffusion model. (b) Plots of $-\ln(1-F)$ vs. time for Cu^{2+} , Pb^{2+} and Ni^{2+} adsorption on NFs, fitted using the Boyd model. Experimental conditions: 20 mg CS-DTPA/PEO NFs, 500 mg L^{-1} initial ion concentration, 150 rpm stirring rate.

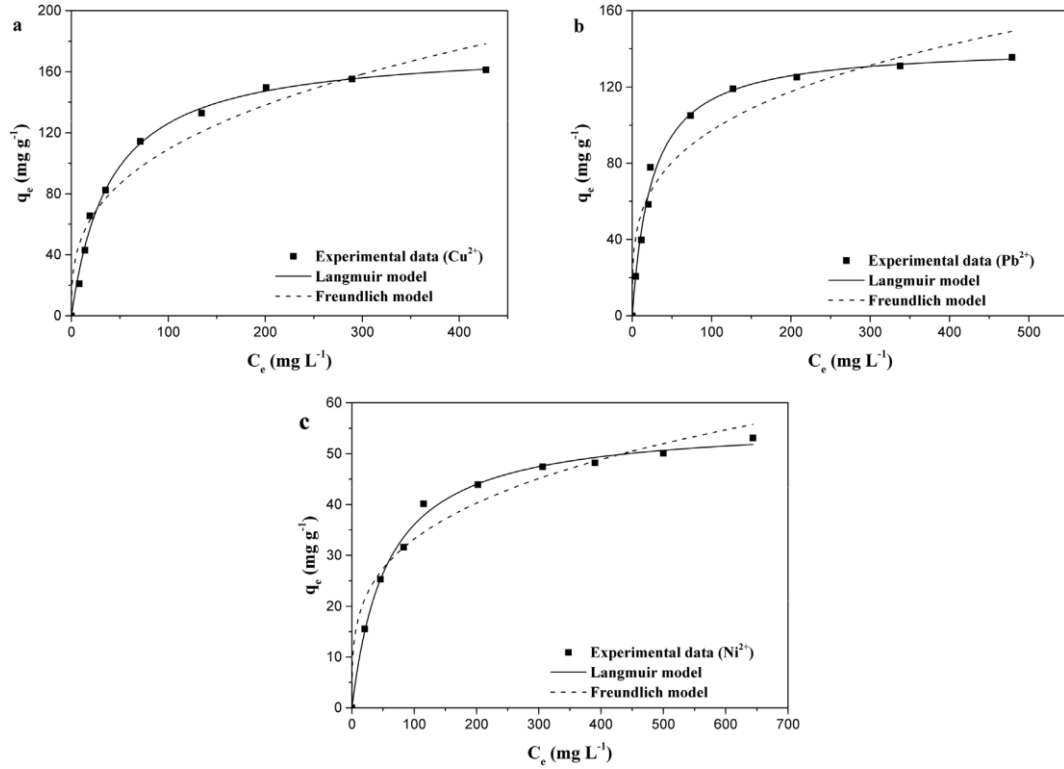


Fig. 8. Equilibrium Cu^{2+} (a), Pb^{2+} (b) and Ni^{2+} (c) uptake capacities of CS-DTPA/PEO NFs (q_e) vs. equilibrium metal ion concentration in solution (C_e) fitted using the Langmuir and Freundlich isotherm models. Experimental conditions: 20 mg CS-DTPA/PEO NFs, 150 rpm stirring rate, 90 min contact time and initial metal ion concentrations ranging from 50 to 750 mg L^{-1} .

Table 3 Correlation coefficient (R^2), isotherm parameters (maximum metal uptake capacity (q_{max}) and equilibrium constants (K_L , K_F , n)) for Cu^{2+} , Pb^{2+} or Ni^{2+} ion adsorption on CS-DTPA/PEO NFs and CS/PEO NFs observed according to the Freundlich and Langmuir isotherm models.

Material (NFs)	Metal	Freundlich isotherm			Langmuir isotherm		
		K_F ($mg\ g^{-1}$)	n	R^2	q_{max} ($mg\ g^{-1}$)	K_L ($L\ mg^{-1}$)	R^2
CS-DTPA/PEO	Cu^{2+}	23	2.9	0.94	177	0.025	0.99
	Pb^{2+}	28	3.6	0.92	142	0.041	0.99
	Ni^{2+}	9	3.6	0.96	56	0.018	0.99
CS/PEO	Cu^{2+}	23	3.3	0.94	144	0.030	0.98
	Pb^{2+}	14	3.1	0.96	113	0.018	0.99
	Ni^{2+}	6	3.1	0.96	50	0.012	0.99

2.7. Evaluation of the regenerative capability of CS-DTPA/PEO nanofibers

To investigate the regenerative capacity of CS-DTPA/PEO nanofibers, five adsorption-desorption cycles were performed. In each step, after Cu^{2+} , Pb^{2+} or Ni^{2+} ion adsorption, CS-DTPA/PEO nanofiber membranes were treated with 10 ml of 0.01 M HNO_3 and 10 ml of 0.01 M $NaOH$ solutions for 5 min and then washed with deionized water up to neutral pH. The optimal contact time for nanofibers contain Cu^{2+} and Ni^{2+} ions were determined experimentally by the loss of color of CS-DTPA/PEO NFs.

3. Results and discussions

3.1. CS-DTPA preparation and characterization

As described above, the presence of a high number of reactive carboxylic groups in DTPA usually leads to chitosan crosslinking, forming insoluble microparticles during the condensation reaction [33]. TEMED/HCl was used as an activation buffer to obtain soluble CS-DTPA with a yield of almost 78% [37], which could undergo further transformations. As previously reported [37,43], the resulting product was analyzed by FTIR (Fig. S1) and 1H NMR (Fig. S2). The presence of typical amide I bond at $1622\ cm^{-1}$ corresponding to C = O stretching vibrations of COOH in carboxylate and amide II and amide III bonds at 1568 and $1390\ cm^{-1}$ corresponding to CN stretching and NH bending vibrations on FTIR spectra of the product (Fig. S1) suggests that DTPA is covalently bound to chitosan [44]. In the 1H NMR spectrum of CS-DTPA (Fig. S2), signals at 4.20 and 2.03 ppm were attributed to protons A of DTPA and protons of acetylated units of chitosan (Hac), respectively. The signals at 3.5-4 ppm were attributed to overlap of C3-C6 protons of chitosan and to B, C protons of DTPA. The peak at 3.20 was related to the overlap of protons D of DTPA and C2 of chitosan.

3.2. Preparation and characterization of CS-DTPA/PEO and CS/PEO nanofibers

The morphology and size distribution of the nanofibers pre- and post-stabilization are illustrated in Fig. 1. Before stabilization, both CS-DTPA/PEO and CS/PEO NFs (Fig. 1 a-b) showed a smooth and uniform surface with fibers averaging 137 and 135 nm in diameter, respectively. Well-known reduction systems, including saturated solutions of K_2CO_3 or $NaOH$ and their mixtures with ethanol, were adopted for nanofibers stabilization [25,39].

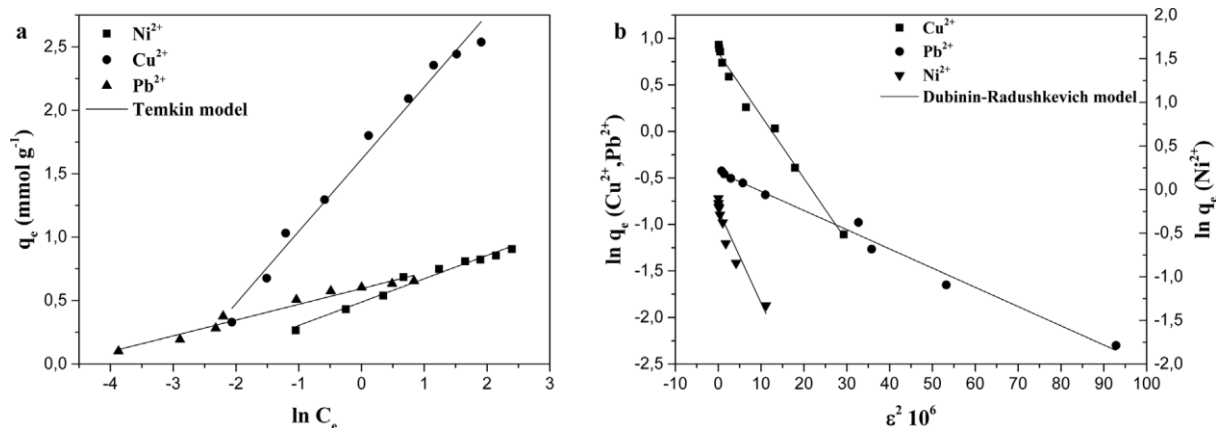


Fig. 9. (a) Plot of the equilibrium Cu^{2+} , Pb^{2+} and Ni^{2+} uptake capacities of CS-DTPA/PEO NFs (q_e) vs. $\ln C_e$ fitted using the Temkin isotherm model. (b) Plot of $\ln q_e$ vs. Polanyi potential ϵ^2 fitted using the Dubinin-Radushkevich isotherm model. Experimental conditions: 20 mg CS-DTPA/PEO NFs, 150 rpm stirring rate and 90 min contact time; the initial metal ion concentrations ranged from 50 to 750 mg L⁻¹.

Table 4 Correlation coefficient (R^2), isotherm parameters (maximum metal uptake capacity (q_{\max}) and isotherm constants (K_T , b , β_{DR} , E) for Cu^{2+} , Pb^{2+} or Ni^{2+} ion adsorption on CS-DTPA/PEO NFs and CS/PEO NFs calculated according to the Temkin and Dubinin-Radushkevich models.

Material (NFs)	Metal ion	Temkin model			Dubinin-Radushkevich model			
		$K_T(\text{L g}^{-1})$	$b(\text{kJ mol}^{-1})$	R^2	$q_{\max}(\text{mmol g}^{-1})$	$\beta_{DR}(\text{mol}^2 \text{J}^{-2})$	$E(\text{kJ mol}^{-1})$	R^2
CS-DTPA/PEO	Cu^{2+}	17.1	4.3	0.97	2.3	$6.7 \cdot 10^{-8}$	2.7	0.98
	Pb^{2+}	121	19.9	0.98	0.7	$2.1 \cdot 10^{-8}$	4.9	0.98
	Ni^{2+}	14.2	13.5	0.97	0.8	$10.6 \cdot 10^{-8}$	2.2	0.91
CS/PEO	Cu^{2+}	23.8	5.7	0.98	1.9	$5.6 \cdot 10^{-8}$	3.0	0.95
	Pb^{2+}	51.3	23.9	0.96	0.4	$2.6 \cdot 10^{-8}$	4.4	0.93
	Ni^{2+}	7.9	14.3	0.97	0.6	$14.4 \cdot 10^{-8}$	1.9	0.85

The reduction process disrupts the nanofiber structure, as shown in **Fig. S3**. To overcome this problem, CS-DTPA/PEO and CS/PEO NFs were preliminarily crosslinked by glutaraldehyde vapor to stabilize the nanofibers before the reduction step. Considering that chitosan reactive $-\text{NH}_2$ groups are implicated in its low crosslinking, the NFs were exposed to 5% glutaraldehyde (GA) for 6 h to preserve the concentration of free amino groups for interaction with metal ions.

As illustrated in the SEM micrographs in **Fig. 1c-d**, the crosslinked CS/PEO and CS-DTPA/PEO NFs preserve their structure and smooth surface after the reduction step. However, CS/PEO and CS-DTPA/PEO NFs display a branched structure and average diameter increased by up to 218 and 180.9 nm, respectively. These features may have resulted from the washing process, which made the nanofibers stick to each other.

The presence of PEO in CS/PEO and CS-DTPA/PEO NFs was observed by ATR-FTIR (**Fig. 2**). The peaks at 2887 and 1563 cm^{-1} can be ascribed to CH_2 stretching and to N-H bending vibrations, respectively, due to crosslinking with PEO and GA. Representative chitosan and chitosan-DTPA functional groups such as N-H and O-H stretching vibrations of the polysaccharide units (3200-3600 cm^{-1}) and C-O-C stretching vibrations at 1100 cm^{-1} are identified in the spectra. The CS-DTPA/PEO structure shows an amide I bond at 1625 cm^{-1} after the stabilization and reduction steps.

X-ray Photoelectron Spectroscopy (XPS) was measured to prove the covalent structure of CS-DTPA/PEO and CS/PEO nanofibers. Wide-scan XPS spectra confirmed the presence of C, N and O

elements. The high-resolution C 1 s and N 1 s spectra are shown in **Fig. 3**. In C 1 s spectra, in XPS spectra of both samples could be found four peaks at 285.0, 286.3, 287.6 and 288.1 eV, corresponding to C-C, C-O/C-N, C = O and O-C = O, respectively. The presence of PEO chains causes high amount of C-O groups. In N1s spectra, peaks at 399.6, 401.0 and 401.9 eV corresponding to C-NH₂ and C-N-C, N-C = O and charged nitrogen N[±] could be found. Successful modification with DTPA was confirmed by higher amount of O-C = O groups originating from DTPA in C 1 s spectra and by higher intensity of peaks corresponding to N-C = O and charged nitrogen in N 1 s spectra of CS-DTPA/PEO.

3.3. Adsorption studies

3.3.1. Optimization of adsorption parameters

The adsorption capacity of CS-DTPA/PEO NFs was assessed for Cu²⁺, Pb²⁺ or Ni²⁺ ions. The color of the nanofibers in contact with Cu²⁺ and Ni²⁺ ions changed during the adsorption process due to the increasing concentration of these ions near the surface of the nanofibers (**Fig. 4a**). As shown in **Fig. 4b**, maintaining the concentration of metal ions constant (300 mg L⁻¹) and varying the [DTPA]/[NH₂] molar ratio significantly increased the adsorption capacity of CS-DTPA/PEO NFs. The trend shows that the optimal [DTPA]/[NH₂] molar ratio is 0.4 (**Fig. 4b**). At higher values, the amount of metal ions adsorbed on the CS-DTPA/PEO NFs does not change significantly.

The effects of pH and initial metal ion concentration on the sorption capacity of CS-DTPA/PEO NFs were investigated (**Fig. 5**) to optimize the conditions of adsorption. The optimal pH range for Cu²⁺, Pb²⁺ or Ni²⁺ ion absorption by CS-DTPA/PEO NFs is from 4 to 6, as shown in **Fig. 5a**. This range is related to the properties of the sorbent and metal salts. After the reduction and washing steps, CS-DTPA/PEO NFs contain free NH₂ and -COOK active groups, which have a high affinity to the metal ions. The presence of -NH₃⁺ and -COOH on the CS-DTPA/PEO NFs surface at low pH causes a strong electrostatic repulsion between them and metal ions in solution, preventing absorption [45]. Raising the pH to 5 promotes a gradual increase in Cu²⁺ and Pb²⁺ absorption, decreasing the impact of the media on the active surface sites [39]. The same trend was been observed for Ni²⁺ when increasing the pH to 6. Further increasing the pH leads to the hydrolysis of metal ions, with the partial formation of metal hydroxides, which are poorly soluble or insoluble in aqueous media, thereby decreasing the adsorption of metal ions by the NH₂ groups [46,47]. As a result, the maximal adsorption capacities of CS-DTPA/PEO NFs was observed at pH 5 for Cu²⁺ and Pb²⁺ ions and at pH 6 for Ni²⁺ ions.

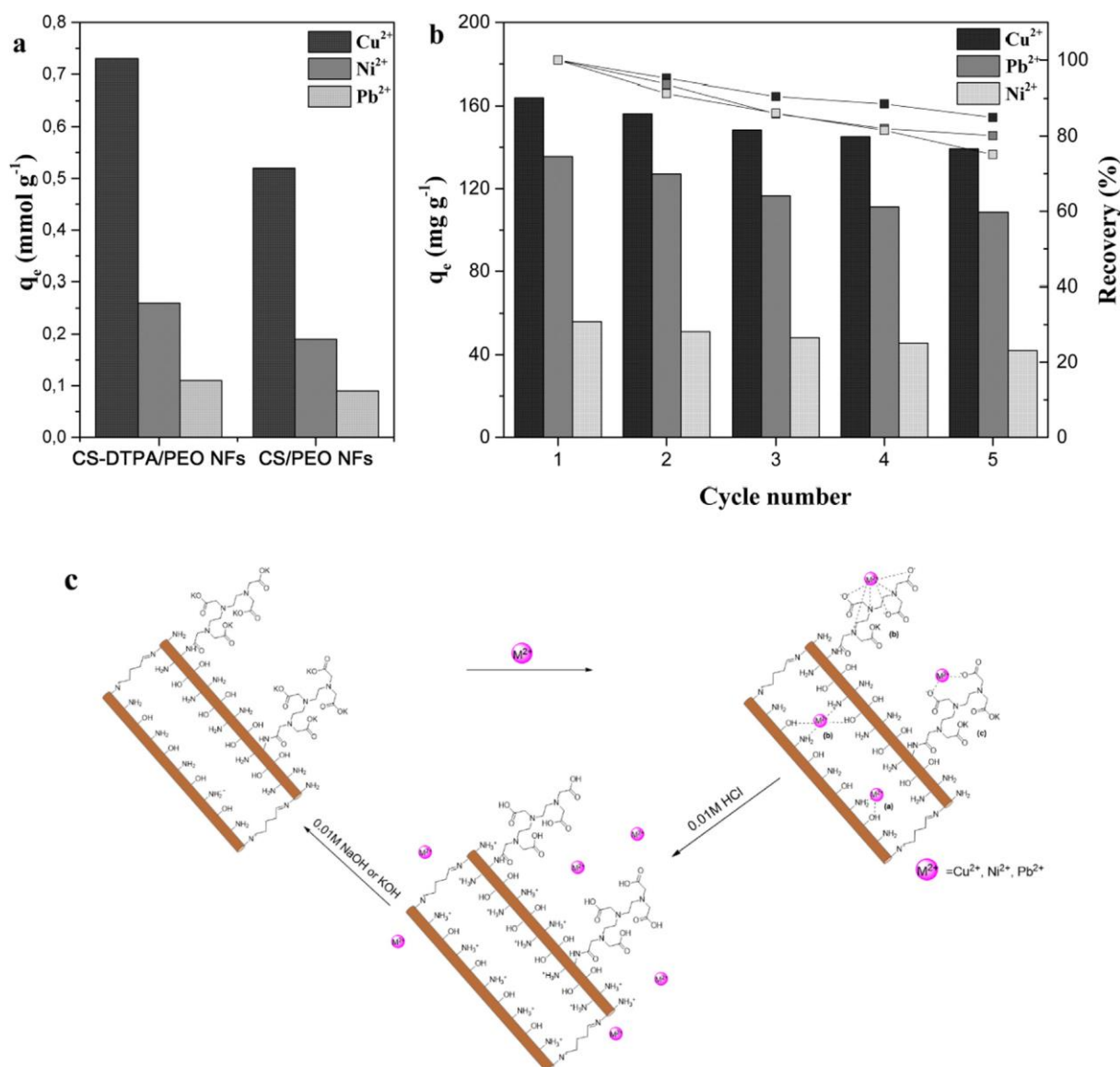


Fig. 10. (a) Competitive Cu , Pb^{2+} and Ni^{2+} adsorption on CS-DTPA/PEO NFs and CS/PEO NFs. Experimental conditions: $\text{pH} = 5$, initial concentrations of metals 200 mg L^{-1} , $100 \text{ mg CS-DTPA/PEO NFs}$ or CS/PEO NFs , 150 rpm stirring rate, 90 min contact time. (b) Cu^{2+} , Pb^{2+} and Ni^{2+} recovery (%) and uptake capacities (q_e) of CS-DTPA/PEO NFs vs adsorption-desorption cycles. Experimental conditions: 500 mg L^{-1} initial metal ion concentration, $20 \text{ mg CS-DTPA/PEO NFs}$, 150 rpm stirring rate, 90 min contact time (c) Possible mechanism of Cu^{2+} , Pb^{2+} and Ni^{2+} adsorption-desorption on CS-DTPA/PEO NFs.

Fig. 5b show the impact of the initial concentrations of the metal ions on the adsorption capacity of CS-DTPA/PEO NFs (initial concentration ranging from 50 to 750 mg L^{-1}). The amount of Cu^{2+} , Pb^{2+} or Ni^{2+} ions adsorbed on the surface of CS-DTPA/PEO NFs increases with the concentrations of the metal ions up to 500 mg L^{-1} . At this concentration, the adsorption capacity of the nanofibers reaches their limit, and a further increasing the metal ion concentrations has no significant effect on the adsorption process, thus indicating the saturation of the active sites. Based on these results, the concentration of Cu^{2+} , Pb^{2+} or Ni^{2+} ions used in subsequent adsorption experiments was 500 mg L^{-1} .

3.3.1.1. Cu^{2+} , Pb^{2+} and Ni^{2+} adsorption kinetics

After performing the experiments at optimal pH and concentration (500 mg L^{-1}), experimental kinetic curves were constructed, as shown in **Fig. 6a**. The amount of Cu^{2+} , Pb^{2+} or Ni^{2+} ions adsorbed on the surface of CS-DTPA/PEO NFs quickly increase 60 min after contact due to the high concentration of active sites on the surface of nanofibers. In the following 30 min, the adsorption rate gradually decreases, reaching the equilibrium after 90 min. Therefore, 90 min can be considered the time at which saturation of the active sites occurs.

To determine the rate-limited step and the adsorption mechanism, pseudo-first-order and pseudo-second-order kinetic, Boyd and intraparticle diffusion models were used to process the experimental data (Eq. (2)-(5)). The patterns of the pseudo-first-order and pseudo-second-order kinetic models for each metal adsorption experiment are illustrated in **Fig. 6b-d**, and the relative kinetic parameters are outlined in **Table 1**. As shown in **Table 1**, the values of equilibrium adsorption capacities for both models match the experimental data. However, the correlation coefficient R^2 of the pseudo-second-order model ($R^2 > 0.99$) is higher than that of the pseudo-first-order model ($R^2 > 0.95$) and, hence, the former is more suitable than the latter. The k_2 constants (**Table 1**) confirm that the Cu^{2+} , Pb^{2+} or Ni^{2+} ions adsorb to the surface of CS-DTPA/PEO NFs at the same rate. According to this model, the rate-limited step of Cu^{2+} , Pb^{2+} or Ni^{2+} ion adsorption is chemisorption, and two active sites on the surface of CS-DTPA/PEO NFs are involved in the adsorption of a single metal ion [48].

The Boyd and intraparticle diffusion models were used to fit experimental adsorption kinetics data (**Fig. 7**) to estimate the contribution of diffusion to the adsorption process [39,49]. As shown in **Fig. 7a**, the adsorption process includes two steps. According to previously published works [50], the second horizontal section of the regression curves (**Fig. 7a**) corresponds to an equilibrium adsorption state and has no effect on adsorption kinetics. As a result, Cu^{2+} , Pb^{2+} and Ni^{2+} adsorption on CS-DTPA/PEO NFs involves a single step, external diffusion, which is characterized by high values of the rate constant K_1 (**Table 2**). As shown in **Fig. 7b**, curve fitted using the Boyd model describes well the kinetics of Cu^{2+} ion adsorption on the surface of nanofibers ($R^2 = 0.99$). However, the rate-kinetic constants (k_b) of this model (**Table 2**) are higher than those of the pseudo-second-order model. Consequently, the ability of the pseudo-second-order model to describe the experimental kinetic data and the adsorption process of Cu^{2+} , Pb^{2+} and Ni^{2+} on CS-DTPA/PEO NFs is limited by the chemisorption step.

3.3.1.2. Adsorption isotherms

It is commonly known that the equilibrium state in adsorption systems primarily depends on the nature of the interaction between adsorbent and adsorbate. The maximum adsorption capacity and equilibrium constant are the main determinants of the optimum mass of adsorbent and of the component profile between adsorbent and water [51].

Herein, Langmuir, Freundlich, Dubinin-Radushkevich and Temkin models were used to describe experimental data on Cu^{2+} , Pb^{2+} or Ni^{2+} ion adsorption on CS-DTPA/PEO NFs. The patterns assessed by fitting the data using the Langmuir and Freundlich models (Eqs. (6) and (7)) and the adsorption parameters are displayed in **Fig. 8** and **Table 3**, respectively. The trend (**Fig. 8**) is more compliant with the Langmuir model than with the Freundlich model, as shown by the correlation coefficients (R^2) (**Table 3**). Moreover, the q_{max} values of CS-DTPA/PEO NFs for Cu^{2+} , Pb^{2+} or Ni^{2+} ion adsorption are 177, 142 and 56 mg g^{-1} , respectively, as determined using the Langmuir model and are in line with the experimental data. Consequently, Cu^{2+} , Pb^{2+} or Ni^{2+} ion adsorption proceeds with the formation of a monomolecular layer on the surface of CS-DTPA/PEO NFs. The results also suggest that active

adsorption sites are homogeneously distributed on the surface of the nanofibers and that free active sites could fix only one Cu^{2+} , Pb^{2+} or Ni^{2+} ion [39].

Although the Langmuir model suggests the formation of a chemical bond between adsorbent and adsorbate, the calculated equilibrium parameters do not provide any information about the nature of this interaction. To describe the physical or chemical nature of the adsorption process, the equilibrium data were processed using the Dubinin-Radushkevich and Temkin isotherm models (Eq. (8) and (9)).

The patterns assessed when using the Dubinin-Radushkevich and Temkin isotherm models are shown in Fig. 9, and the related adsorption parameters are outlined in Table 4. The values of the Temkin coefficient b related to adsorption heat and the calculated values of free adsorption energy (Eq. (10) and Table 4) are lower than 80 kJ mol^{-1} and 8 kJ mol^{-1} , respectively, thus indicating that Cu^{2+} , Pb^{2+} and Ni^{2+} ion adsorption on CS-DTPA/PEO NFs primarily depends on physical interactions [26,42].

The same equilibrium experiments were performed for CS/PEO NFs (Fig. S4). The comparison of data of CS/PEO NFs with those of CS-DTPA/PEO NFs (Table 3) shows that the presence of functional groups of DTPA increases the maximum adsorption capacity of Cu^{2+} , Pb^{2+} and Ni^{2+} ions on the surface of the nanofibers by 22.8, 25.7 and 14%, respectively. However, the additional active sites do not affect the mechanism of adsorption, which is also physical for pure nanofibers (Table 4).

Most importantly, CS-DTPA/PEO NFs also have a higher capacity to adsorb Cu^{2+} , Pb^{2+} and Ni^{2+} ions than other known chitosan-based and modified chitosan-based adsorbents (Table S1) [33,52,53,54].

3.4. Competitive adsorption

Competitive adsorption studies allowed us to determine the relevant selectivity of CS-DTPA/PEO NFs to metal ions in multicomponent systems. As shown in Fig. 10a, CS-DTPA/PEO NFs have a higher ability to adsorb Cu^{2+} than Ni^{2+} or Pb^{2+} ions in their mixture. Simultaneously, the findings are in line with the stability constant of complexes of these metal ions with chitosan, O-containing-chitosan derivatives and DTPA (EDTA), which decrease in the series: $\text{Cu}^{2+} > \text{Ni}^{2+} > \text{Pb}^{2+}$ [52,55]. Thus, additional functional groups from DTPA improve the adsorption properties of CS-DTPA/PEO NFs but do not affect the selectivity of the material.

3.5. Regeneration studies of CS-DTPA/PEO NFs and adsorption-desorption mechanism

Regeneration and reusability are essential properties of any adsorbent. For CS-DTPA/PEO NFs, 5 sequential adsorption-desorption cycles were performed to assess the regenerative capacity and the loss of activity after each cycle. As shown in Fig. 10b, after 5 adsorption-desorption cycles, the adsorption capacity of CS-DTPA/PEO NFs for Cu^{2+} , Pb^{2+} and Ni^{2+} ions decreased by 17, 20 and 12%, respectively. This decrease can be explained by the reduction in the number of available active sites as the nanofibers stick to each other (Fig. S5) during the regeneration process. However, the nanofibrous structure and the high sorption capacity of CS-DTPA/PEO NFs remain unchanged after five regeneration cycles.

Based on adsorption and regeneration studies, the possible adsorption-desorption mechanism is shown in Fig. 10c. CS-DTPA/PEO NFs effectively remove Cu^{2+} , Pb^{2+} and Ni^{2+} ions from aqueous solution thanks to the synergistic effect of the active $-\text{COO}-$ and free $-\text{NH}_2$ and $-\text{OH}$ groups on their surface, which determine the adsorption properties of each component in the adsorbent. Generally, Cu^{2+} , Pb^{2+} and Ni^{2+} retention on the surface of CS-DTPA/PEO NFs is associated with (a) electrostatic attractions

between metal ions and -OH and NH₂ groups of the chitosan fragment, (b) coordination of divalent metals with DTPA fragments and NH₂ groups of chitosan and (c) leaching of K or Na ions from two carboxylate anions of DTPA fragments (**Fig. 9c**) [36,56]. According to adsorption isotherms studies (Section 3.3.3.), electrostatic interaction and leaching processes are more prevalent during the adsorption. Physical adsorption was also confirmed by the fast desorption of Cu²⁺, Pb²⁺ and Ni²⁺ ions from CS-DTPA/PEO NFs after treatment with slightly acidic solutions (0.01 M HCl), which protonated -NH₂ and -COO⁻ groups and led to repulsion between these groups and metal ions. Further treatment of CS-DTPA/PEO NFs with NaOH solution neutralized the excess of acid and activated the -NH₂ and -COONa groups on the surface for the next adsorption cycle.

4. Conclusion

In the present study, a series of CS-DTPA/PEO electrospun nanofiber membranes were successfully prepared for the effective removal of Cu²⁺, Pb²⁺ and Ni²⁺ ions from aqueous solutions. Batch adsorption experiments showed that the adsorption capacity of CS-DTPA/PEO NFs for metal ions decreases in the series: Cu²⁺ > Pb²⁺ > Ni²⁺. A pseudofirst-order model describes adsorption kinetic data, and the adsorption of one Cu²⁺, Pb²⁺ or Ni²⁺ ion require two active centers. Adsorption isotherm analysis showed that the adsorption process is closest to the Langmuir model and proceeds with the formation of a monomolecular layer on the surface of CS-DTPA/PEO NFs. Based on the Langmuir model, the maximum adsorption capacities of CS-DTPA/PEO NFs for Cu²⁺, Pb²⁺ and Ni²⁺ are 177, 142 and 56 mg g⁻¹, respectively. The calculated adsorption heat and free energy values based on the Temkin and Dubinin-Radushkevich models, respectively, indicate the physical nature of Cu²⁺, Pb²⁺ or Ni²⁺ ion adsorption on CS-DTPA/PEO NFs. In addition, several adsorption-desorption experiments showed that CS-DTPA/PEO NFs have excellent regenerative capability and reusability, with a slight decrease in the adsorption capacity of the material after 5 cycles.

References

- [1] V. Karri, M. Schuhmacher, V. Kumar, Heavy metals (Pb, Cd, As and MeHg) as risk factors for cognitive dysfunction: A general review of metal mixture mechanism in brain, *Environ. Toxicol. Pharmacol.* 48 (2016) 203-213, <https://doi.org/10.1016/j.etap.2016.09.016>.
- [2] L. Chen, S. Zhou, Y. Shi, C. Wang, B. Li, Y. Li, S. Wu, Heavy metals in food crops, soil, and water in the Lihe River Watershed of the Taihu Region and their potential health risks when ingested, *Sci. Total Environ.* 615 (2018) 141-149, <https://doi.org/10.1016/j.scitotenv.2017.09.230>.
- [3] K. Rehman, F. Fatima, I. Waheed, M.S.H. Akash, Prevalence of exposure of heavy metals and their impact on health consequences, *J. Cell. Biochem.* 119 (2018) 157-184, <https://doi.org/10.1002/jcb.26234>.
- [4] M. Jaishankar, T. Tseten, N. Anbalagan, B.B. Mathew, K.N. Beeregowda, Toxicity, mechanism and health effects of some heavy metals, *Interdiscip. Toxicol.* 7 (2014) 60-72, <https://doi.org/10.2478/intox-2014-0009>.
- [5] L.M. Chiesa, F. Ceriani, M. Caligara, D. Di Candia, R. Malandra, S. Panseri, F. Arioli, Mussels and clams from the Italian fish market. Is there a human exposure risk to metals and arsenic? *Chemosphere* 194 (2018) 644-649, <https://doi.org/10.1016/j.chemosphere.2017.12.041>.

- [6] S. Paz, C. Rubio, I. Frías, Á.J. Gutiérrez, D. González-Weller, V. Martín, C. Revert, A. Hardisson, Toxic metals (Al, Cd, Pb and Hg) in the most consumed edible seaweeds in Europe, *Chemosphere* (2019) 879-884, <https://doi.org/10.1016/jLchemosphere.2018.11.165>.
- [7] R. Singh, N. Gautam, A. Mishra, R. Gupta, Heavy metals and living systems: An overview, *Indian J. Pharmacol.* 43 (2011) 246-253, <https://doi.org/10.4103/0253-7613.81505>.
- [8] S. Sobhanardakani, L. Tayebi, S.V. Hosseini, Health risk assessment of arsenic and heavy metals (Cd, Cu Co, Pb, and Sn) through consumption of caviar of *Acipenser persicus* from Southern Caspian Sea, *Environ. Sci. Pollut. Res.* 25 (2018) 2664-2671, <https://doi.org/10.1007/s11356-017-0705-8>.
- [9] N.B. Singh, G. Nagpal, S. Agrawal, Rachna, Water purification by using Adsorbents: A Review, *Environ. Technol. Innov.* 11 (2018) 187-240, <https://doi.org/10.1016/jLeti.2018.05.006>.
- [10] V.K. Sharma, T.J. McDonald, H. Kim, V.K. Garg, Magnetic graphene-carbon nanotube iron nanocomposites as adsorbents and antibacterial agents for water purification, *Adv. Colloid Interface Sci.* 225 (2015) 229-240, <https://doi.org/10.1016/j.cis.2015.10.006>.
- [11] M.F. Hamza, J.C. Roux, E. Guibal, Uranium and europium sorption on amidoxime-functionalized magnetic chitosan micro-particles, *Chem. Eng. J.* 344 (2018) 124-137, <https://doi.org/10.1016/jLcej.2018.03.029>.
- [12] G. Zhao, X. Huang, Z. Tang, Q. Huang, F. Niu, X. Wang, Polymer-based nanocomposites for heavy metal ions removal from aqueous solution: A review, *Polym. Chem.* 9 (2018) 3562-3582, <https://doi.org/10.1039/c8py00484f>.
- [13] Y. Wu, H. Pang, Y. Liu, X. Wang, S. Yu, D. Fu, J. Chen, X. Wang, Environmental remediation of heavy metal ions by novel-nanomaterials: A review, *Environ. Pollut.* (2019) 608-620, <https://doi.org/10.1016/jLenvpol.2018.12.076>.
- [14] G. Zhou, J. Luo, C. Liu, L. Chu, J. Crittenden, Efficient heavy metal removal from industrial melting effluent using fixed-bed process based on porous hydrogel adsorbents, *Water Res.* 131 (2018) 246-254, <https://doi.org/10.1016/jLwatres.2017.12.067>.
- [15] D. Morillo Martín, M. Faccini, M.A. García, D. Amantia, Highly efficient removal of heavy metal ions from polluted water using ion-selective polyacrylonitrile nanofibers, *J. Environ. Chem. Eng.* 6 (2018) 236-245, <https://doi.org/10.1016/jLjece.2017.11.073>.
- [16] K. Zhang, Z. Li, N. Deng, J. Ju, Y. Li, B. Cheng, W. Kang, J. Yan, Tree-like cellulose nanofiber membranes modified by citric acid for heavy metal ion (Cu²⁺) removal, *Cellulose* 26 (2019) 945-958, <https://doi.org/10.1007/s10570-018-2138-z>.
- [17] A. Kolbasov, S. Sinha-Ray, A.L. Yarin, B. Pourdeyhimi, Heavy metal adsorption on solution-blown biopolymer nano fiber membranes, *J. Memb. Sci.* 530 (2017) 250-263, <https://doi.org/10.1016/jLmemsci.2017.02.019>.
- [18] G. Kummer, C. Schonhart, M.G. Fernandes, G.L. Dotto, A.L. Missio, D.A. Bertuol, E.H. Tanabe, Development of Nanofibers Composed of Chitosan/Nylon 6 and Tannin/Nylon 6 for Effective Adsorption of Cr(VI), *J. Polym. Environ.* 26 (2018) 4073-4084, <https://doi.org/10.1007/s10924-018-1281-9>.

- [19] H. Beheshti, M. Irani, L. Hosseini, A. Rahimi, M. Aliabadi, Removal of Cr (VI) from aqueous solutions using chitosan/MWCNT/Fe₃O₄ composite nanofibers-batch and column studies, *Chem. Eng. J.* 284 (2016) 557-564, <https://doi.org/10.1016/j.lcej.2015.08.158>.
- [20] M. Jiang, T. Han, J. Wang, L. Shao, C. Qi, X.M. Zhang, C. Liu, X. Liu, Removal of heavy metal chromium using cross-linked chitosan composite nanofiber mats, *Int. J. Biol. Macromol.* 120 (2018) 213-221, <https://doi.org/10.1016/j.ijbiomac.2018.08.071>.
- [21] M.I. Shariful, S. Bin Sharif, J.J.L. Lee, U. Habiba, B.C. Ang, M.A. Amalina, Adsorption of divalent heavy metal ion by mesoporous-high surface area chitosan/ poly (ethylene oxide) nanofibrous membrane, *Carbohydr. Polym.* 157 (2017) 57-64. <https://doi.org/10.1016/j.carbpol.2016.09.063>.
- [22] P. Kanmani, J. Aravind, M. Kamaraj, P. Sureshbabu, S. Karthikeyan, Environmental applications of chitosan and cellulosic biopolymers: A comprehensive outlook, *Bioresour. Technol.* 242 (2017) 295-303, <https://doi.org/10.1016/j.lbiortech.2017.03.119>.
- [23] W.S. Wan Ngah, L.C. Teong, M.A.K.M. Hanafiah, Adsorption of dyes and heavy metal ions by chitosan composites: A review, *Carbohydr. Polym.* 83 (4) (2011) 1446-1456, <https://doi.org/10.1016/j.lcarbpol.2010.11.004>.
- [24] K. Yang, G. Wang, X. Chen, X. Wang, F. Liu, Treatment of wastewater containing Cu²⁺ using a novel macromolecular heavy metal chelating flocculant xanthated chitosan, *Colloids Surfaces A Physicochem. Eng. Asp.* 558 (2018) 384-391, <https://doi.org/10.1016/j.colsurfa.2018.06.082>.
- [25] S.M. Lemma, F. Bossard, M. Rinaudo, Preparation of pure and stable chitosan nanofibers by electrospinning in the presence of poly(ethylene oxide), *Int. J. Mol. Sci.* 17 (2016) 1790, <https://doi.org/10.3390/ijms17111790>.
- [26] M. Aliabadi, M. Irani, J. Ismaeili, H. Piri, M.J. Parnian, Electrospun nanofiber membrane of PEO/Chitosan for the adsorption of nickel, cadmium, lead and copper ions from aqueous solution, *Chem. Eng. J.* 220 (2013) 237-243, <https://doi.org/10.1016/j.cej.2013.01.021>.
- [27] L. Zhang, Y. Zeng, Z. Cheng, Removal of heavy metal ions using chitosan and modified chitosan: A review, *J. Mol. Liq.* 214 (2016) 175-191, <https://doi.org/10.1016/j.molliq.2015.12.013>.
- [28] J. Wang, C. Chen, Chitosan-based biosorbents: Modification and application for biosorption of heavy metals and radionuclides, *Bioresour. Technol.* 160 (2014) 129-141, <https://doi.org/10.1016/j.lbiortech.2013.12.110>.
- [29] Y. Lin, Y. Hong, Q. Song, Z. Zhang, J. Gao, T. Tao, Highly efficient removal of copper ions from water using poly(acrylic acid)-grafted chitosan adsorbent, *Colloid Polym. Sci.* 295 (2017) 627-635, <https://doi.org/10.1007/s00396-017-4042-8>.
- [30] H. Yan, J. Dai, Z. Yang, H. Yang, R. Cheng, Enhanced and selective adsorption of copper(II) ions on surface carboxymethylated chitosan hydrogel beads, *Chem. Eng. J.* 174 (2011) 586-594, <https://doi.org/10.1016/j.lcej.2011.09.064>.
- [31] M.T. Friend, N.A. Wall, Stability constants for Zirconium(IV) complexes with EDTA, CDTA, and DTPA in perchloric acid solutions, *Inorganica Chim. Acta.* 484 (2019) 357-367, <https://doi.org/10.1016/j.lica.2018.09.034>.

- [32] E. Repo, L. Malinen, R. Koivula, R. Harjula, M. Sillanpaa, Capture of Co(II) from its aqueous EDTA-chelate by DTPA-modified silica gel and chitosan, *J. Hazard. Mater.* 187 (2011) 122-132, <https://doi.org/10.1016/j.jlhazmat.2010.12.113>.
- [33] E. Repo, J.K. Warchol, T.A. Kurniawan, M.E.T. Sillanpaa, Adsorption of Co(II) and Ni(II) by EDTA- and/or DTPA-modified chitosan: Kinetic and equilibrium modeling, *Chem. Eng. J.* 161 (2010) 73-82, <https://doi.org/10.1016/j.lcej.2010.04.030>.
- [34] Y. Huang, H. Wu, T. Shao, X. Zhao, H. Peng, Y. Gong, H. Wan, Enhanced copper adsorption by DTPA-chitosan/alginate composite beads: Mechanism and application in simulated electroplating wastewater, *Chem. Eng. J.* 339 (2018) 322-333, <https://doi.org/10.1016/j.lcej.2018.01.071>.
- [35] F. Zhao, E. Repo, M. Sillanpaa, Y. Meng, D. Yin, W.Z. Tang, Green synthesis of magnetic EDTA- And/or DTPA-cross-linked chitosan adsorbents for highly efficient removal of metals, *Ind. Eng. Chem. Res.* 54 (2015) 1271-1281, <https://doi.org/10.1021/ie503874x>.
- [36] D. Wu, L. Hu, Y. Wang, Q. Wei, L. Yan, T. Yan, Y. Li, B. Du, EDTA modified p-cyclodextrin/chitosan for rapid removal of Pb(II) and acid red from aqueous solution, *J. Colloid Interface Sci.* 523 (2018) 56-64, <https://doi.org/10.1016/j.jcis.2018.03.080>.
- [37] V. Darras, M. Nelea, F.M. Winnik, M.D. Buschmann, Chitosan modified with gadolinium diethylenetriaminepentaacetic acid for magnetic resonance imaging of DNA/chitosan nanoparticles, *Carbohydr. Polym.* 80 (2010) 1137-1146, <https://doi.org/10.1016/j.carbpol.2010.01.035>.
- [38] L. Zeng, Y. Chen, Q. Zhang, X. Guo, Y. Peng, H. Xiao, X. Chen, J. Luo, Adsorption of Cd(II), Cu(II) and Ni(II) ions by cross-linking chitosan/rectorite nano-hybrid composite microspheres, *Carbohydr. Polym.* 130 (2015) 333-343, <https://doi.org/10.1016/j.carbpol.2015.05.015>.
- [39] D. Yang, L. Li, B. Chen, S. Shi, J. Nie, G. Ma, Functionalized chitosan electrospun nanofiber membranes for heavy-metal removal, *Polymer.* 163 (2019) 74-85, <https://doi.org/10.1016/j.polymer.2018.12.046>.
- [40] J.P. Simonin, On the comparison of pseudo-first order and pseudo-second order rate laws in the modeling of adsorption kinetics, *Chem. Eng. J.* 300 (2016) 254-263, <https://doi.org/10.1016/j.cej.2016.04.079>.
- [41] N. Ayawei, A.N. Ebelegi, D. Wankasi, Modelling and Interpretation of Adsorption Isotherms, *J. Chem.* 2017 (2017) 1-11, <https://doi.org/10.1155/2017/3039817>.
- [42] E. Inam, U.J. Etim, E.G. Akpabio, S.A. Umoren, Process optimization for the application of carbon from plantain peels in dye abstraction, *J. Taibah Univ. Sci.* 11 (2016) 173-185, <https://doi.org/10.1016/j.jtusci.2016.01.003>.
- [43] L. Zhang, T. Liu, Y. Xiao, D. Yu, N. Zhang, Hyaluronic Acid-Chitosan Nanoparticles to Deliver Gd-DTPA for MR Cancer Imaging, *Nanomaterials.* 5 (2015) 1379-1396, <https://doi.org/10.3390/nano5031379>.
- [44] J. Kong, S. Yu, Fourier transform infrared spectroscopic analysis of protein secondary structures, *Acta Biochim. Biophys. Sin.* 39 (2007) 549-559, <https://doi.org/10.1111/j.1745-7270.2007.00320.x>.

- [45] A. Kong, Y. Ji, H. Ma, Y. Song, B. He, J. Li, A novel route for the removal of Cu(II) and Ni(II) ions via homogeneous adsorption by chitosan solution, *J. Clean. Prod.* 192 (2018) 801-808, <https://doi.org/10.1016/j.jclepro.2018.04.271>.
- [46] F. Einollahi Peer, N. Bahramifar, H. Younesi, Removal of Cd (II), Pb (II) and Cu (II) ions from aqueous solution by polyamidoamine dendrimer grafted magnetic graphene oxide nanosheets, *J. Taiwan Inst. Chem. Eng.* 87 (2018) 225-240, <https://doi.org/10.1016/j.jtice.2018.03.039>.
- [47] S.A. Kosa, G. Al-Zhrani, M. Abdel Salam, Removal of heavy metals from aqueous solutions by multi-walled carbon nanotubes modified with 8-hydroxyquinoline, *Chem. Eng. J.* 181-182 (2012) 159-168, <https://doi.org/10.1016/j.cej.2011.11.044>.
- [48] M.R. Karim, M.O. Aijaz, N.H. Alharth, H.F. Alharbi, F.S. Al-Mubaddel, M.R. Aual, Composite nanofibers membranes of poly(vinyl alcohol)/chitosan for selective lead (II) and cadmium(II) ions removal from wastewater, *Ecotoxicol. Environ. Saf.* 169 (2019) 479-486, <https://doi.org/10.1016/j.ecoenv.2018.11.049>.
- [49] A.B. Albadarin, M.N. Collins, M. Naushad, S. Shirazian, G. Walker, C. Mangwandi, Activated lignin-chitosan extruded blends for efficient adsorption of methylene blue, *Chem. Eng. J.* 307 (2017) 264-272, <https://doi.org/10.1016/j.cej.2016.08.089>.
- [50] E. Da'na, A. Sayari, Adsorption of copper on amine-functionalized SBA-15 prepared by co-condensation: Equilibrium properties, *Chem. Eng. J.* 166 (2011) 445-453. <https://doi.org/10.1016/j.cej.2010.11.016>.
- [51] S.P.D. Monte Blanco, F.B. Scheufele, A.N. Módenes, F.R. Espinoza-Quiñones, P. Marin, A.D. Kroumov, C.E. Borba, Kinetic, equilibrium and thermodynamic phenomenological modeling of reactive dye adsorption onto polymeric adsorbent, *Chem. Eng. J.* 307 (2017) 466-475. <https://doi.org/10.1016/j.cej.2016.08.104>.
- [52] J. Ma, G. Zhou, L. Chu, Y. Liu, C. Liu, S. Luo, Y. Wei, Efficient Removal of Heavy Metal Ions with An EDTA Functionalized Chitosan/Polyacrylamide Double Network Hydrogel, *ACS Sustain. Chem. Eng.* 5 (2017) 843-851, <https://doi.org/10.1021/acssuschemeng.6b02181>.
- [53] I. Lakhdhar, P. Mangin, B. Chabot, Copper (II) ions adsorption from aqueous solutions using electrospun chitosan/peo nanofibres: Effects of process variables and process optimization, *J. Water Process Eng.* 7 (2015) 295-305, <https://doi.org/10.1016/j.jwpe.2015.07.004>.
- [54] X. Luo, J. Zeng, S. Liu, L. Zhang, An effective and recyclable adsorbent for the removal of heavy metal ions from aqueous system: Magnetic chitosan/cellulose microspheres, *Bioresour. Technol.* 194 (2015) 403-406, <https://doi.org/10.1016/j.biortech.2015.07.044>.
- [55] A. Pestov, S. Bratskaya, Chitosan and its derivatives as highly efficient polymer ligands, *Molecules* 21 (2016) 330, <https://doi.org/10.3390/molecules21030330>.
- [56] J.R.B. Gomes, M. Jorge, P. Gomes, Interaction of chitosan and chitin with Ni, Cu and Zn ions: A computational study, *J. Chem. Thermodyn.* 73 (2014) 121-129, <https://doi.org/10.1016/j.jct.2013.11.016>.